Monte Carlo simulation of two-dimensional hard rectangles: Confinement effects

Derek A. Triplett[1] and Kristen A. Fichthorn[1,2,*]

[1]*Department of Chemical Engineering, The Pennsylvania State University, University Park, Pennsylvania 16802, USA*

[2]*Department of Physics, The Pennsylvania State University, University Park, Pennsylvania 16802, USA*

(Received 3 August 2007; revised manuscript received 24 September 2007; published 31 January 2008)

We use orientational-bias Monte Carlo simulations to examine the phase behavior of two-dimensional hard rectangles in the bulk and under confinement by hard walls. For all of the rod aspect ratios and area fractions studied, we find that confinement increases the degree of nematic ordering over the bulk, as confined rods tend to align their long axes parallel to the confining walls. The extent of nematic ordering increases as the separation between the confining walls decreases. If the aspect ratio of the rectangles is sufficiently large, they exhibit nematic ordering in both the bulk and under confinement, where the nematic director is set by the walls. Rods with a small aspect ratio are isotropic in the bulk and exhibit weak tetratic tendencies for sufficiently high densities. From studies of density profiles, angular distributions, and orientational correlation functions for confined, low-aspect-ratio rods, it is apparent that they align their long axes parallel to the wall in the near-wall region, where layering occurs for sufficiently high rod densities. However, confined rods with low aspect ratios still exhibit weak tetratic (isotropic) tendencies near the center of the confined region for all but the smallest wall separations. We note that although our studies probe the ordering of hard rectangles, the entropic tendencies that we observe here will be present for rods with energetic interactions. Thus, these studies serve as a general starting point for understanding and controlling the assembly of rods in two-dimensional confining geometries.

DOI: 10.1103/PhysRevE.77.011707 PACS number(s): 61.30.Hn, 61.25.−f, 61.30.Pq, 61.20.Ja

I. INTRODUCTION

Understanding and controlling the two and three-dimensional assembly of nanowires is pertinent to the bottom-up fabrication of nanoelectronic circuits [1–6] and sensors [7]. From a fundamental perspective, the phase behavior of rodlike entities is surprisingly diverse and still not fully understood. Here, we focus on hard rods, which have only excluded-volume interactions with one another. Studies of hard rods yield insight into entropic effects associated with a rodlike shape and are, thus, useful in understanding suspensions of rods with energetic interactions, as well. Much work has been done to develop an understanding of the various phases exhibited by hard-rod fluids in two [8–15] and three [16–22] dimensions. Onsager determined that when the density is increased in a system of three-dimensional hard rods, the rods transition from a low-density, isotropic phase, in which they have no preferred alignment, to a nematic phase, in which they are orientationally aligned [16]. The isotropic and nematic phases are observed for most rodlike entities in three dimensions if the aspect ratio (the ratio of their length to width) is sufficiently high. However, other phases can be observed in rods with low aspect ratios. For example, studies of short cylinders [17] and cuboids [18] have explored the possibility of a cubatic phase [17–19], in which the particles have long-range orientational order with cubic symmetry, but lack positional order. In simulations of cuboids [18] and spherocylinders [20], as well as in experimental studies of *fd* virus particles [21], smectic phases have been observed. For spherocylinders and cuboids, the existence of the smectic phase was shown to depend on the aspect ratio [18,20]. In two dimensions, studies have probed the phase behavior of spherocylinders [8,9], rectangles [8,10], ellipses [11,12], and needles [13,14]. The isotropic-to-nematic transition has been observed with increasing density in theoretical studies of rectangles [8], spherocylinders [8], and ellipses [11], as well as in simulations of spherocylinders [9], ellipses [12], and needles [13,14]. If the density is sufficiently high, a transition from the nematic to the solid (smectic) phase occurs for spherocylinders with aspect ratios $\gtrsim 7$ [9]. Two-dimensional simulation studies of low-aspect-ratio rectangles [8,10] have explored the possibility of the tetratic phase in which small domains of rectangles align perpendicular to each other.

To be able to exploit the ordering of rods for certain applications (e.g., nanoelectronic circuits), it is desirable to confine them in nanoscale geometries on surfaces. Such confinement can be achieved by patterning the surface, either physically [3] or chemically [4,5]. Experiments with Langmuir-Blodgett troughs have been useful at probing rod ordering in quasi-two-dimensional confined systems [1,23–27]. Simulation studies have also explored the ordering and phase behavior of rods under confinement by hard walls in two [28] and three [29–32,34] dimensions, as well as in quasi-two-dimensional slit-pore geometries [33,35,36]. A typical finding in such studies is that hard walls induce rods to align with their long axes parallel to the walls. For example, studies of spherocylinders in quasi-two-dimensional slits have demonstrated that the spherocylinders align with their long axes parallel to the slit walls and exhibit an isotropic to nematic transition with increasing density [35]. In studies involving spherocylinders near a single hard wall, Dijkstra *et al.* observed alignment in biaxial domains with rod axes parallel to the wall. They also observed that the distance over which rods maintain their parallel alignment with the wall increases with increasing density [30].

*fichthorn@psu.edu

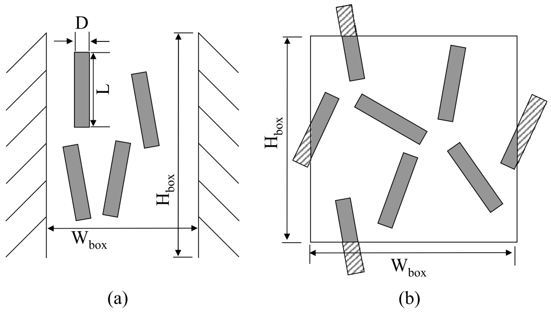

FIG. 1. Example simulation box of (a) a confined system and (b) a bulk system. L and D are the length and width of the rectangles, respectively, while H_{box} and W_{box} are the height and width of the simulation box, respectively. The lightly shaded portions of the rods shown in (b) reflect the periodic boundary conditions used.

Martínez-Ratón explored the effect of confinement on short rectangles in two dimensions and reported extensive layering near the wall [28].

Our interest lies in understanding the extent to which hard walls influence rod alignment in two dimensions. In particular, we study two-dimensional hard rectangles confined between hard walls that are infinitely long, but spaced a finite distance apart. Based on the results of previous studies [28–33,35], we expect (and find) that rectangles near the walls orient their long axes parallel to the walls. The wall orientation effect occurs even for rods that exhibit tetratic tendencies in the bulk. The orientations of rods near the walls are surprisingly similar (but not completely identical) to those of rods near other rods in the bulk. We demonstrate that we can exploit the wall effect to achieve confined nematics at densities for which the bulk phase is isotropic.

II. MODELS AND METHODS

We study the phase behavior of two-dimensional hard rods confined between hard walls and in bulk. Figure 1 illustrates the essential elements of the confined and bulk systems. The rods are modeled as two-dimensional rectangles having a length L, a width D, and an aspect ratio of $\alpha = L/D$. In the confined systems, the distance between the walls is given by W_{box}. We studied $W_{\text{box}}=L$, $2L$, $5L$, and $10L$. The length parallel to the confining walls is given by H_{box}, which we set to be a minimum of $10L$ to avoid finite-size effects. We verified that doubling the value of H_{box} in the confined systems had no measurable effect on the results. Periodic boundary conditions were enforced parallel to the walls to give the effect of infinitely long, hard barriers. In the bulk systems $H_{\text{box}}=W_{\text{box}}$, which ranges from $W_{\text{box}}=10L$ to $W_{\text{box}}=26L$, and periodic boundary conditions were applied in both directions. For low rod densities, these box sizes are larger than rod-rod correlation lengths. However, for the highest rod densities, where nematic phases are present, rod-rod correlation lengths exceed the box size. We studied rods with aspect ratios of $\alpha=7.5$, 13.3, and 20.0. For each of these aspect ratios we probed fractional coverages of $A_f=0.4$, 0.6, and 0.7, where the fractional coverage is defined as

$$A_f = \frac{N_{\text{rods}} L D}{H_{\text{box}} W_{\text{box}}}, \qquad (1)$$

and N_{rods} is the number of rods in the system. The number of rods ranges from 80, for confined systems with $W_{\text{box}}=L$, to 3200 for bulk simulations.

To probe the phase behavior, we used orientational-bias Monte Carlo (MC) simulations [37], which we found to be more efficient than conventional Metropolis MC simulations. In orientational-bias MC simulations, multiple trial angles of a rod are attempted for a given center-of-mass displacement. Here, a trial move consists of a random center-of-mass displacement with a maximum distance of D. For a given center-of-mass displacement, ten trial angles, ranging between 0° and 179° are randomly attempted about the rod's new and old center of mass. In both the new and old center of mass locations, the Rosenbluth factor W is calculated as

$$W = \sum_{j=1}^{k} \exp[-\beta U^{\text{or}}(b_j)]. \qquad (2)$$

Here k is the number of trial orientations, b_j is a specific trial orientation, U^{or} is the energy of the orientation, and $\beta = (k_B T)^{-1}$. The energy U^{or} is given by a hard-core potential, i.e., $U^{\text{or}}=\infty$, if two rods overlap and $U^{\text{or}}=0$, otherwise. The rods also interact with the walls via a hard-core potential, i.e., $U^{\text{or}}=\infty$, if a rod overlaps with a wall. Out of the k orientations in the new location with W_{new}, a particular orientation b_n is selected with a probability given by

$$P(b_n) = \frac{\exp[-\beta U^{\text{or}}(b_n)]}{W_{\text{new}}}. \qquad (3)$$

The probability of accepting the move $P_{\text{old}\rightarrow\text{new}}$ is given by

$$P_{\text{old}\rightarrow\text{new}} = \min\left(1, \frac{W_{\text{new}}}{W_{\text{old}}}\right). \qquad (4)$$

A uniform random number ran$X$ is generated. If ran$X$ is less than $P_{\text{old}\rightarrow\text{new}}$ the move is accepted, otherwise the move is rejected. The average acceptance rate of trial moves is typically 20% but can vary from a minimum of 5%, for the simulations with high A_f, to a maximum of 35% for low A_f.

These simulations were performed on-lattice, so that the rods are represented by discrete points on a grid. It was shown by Panagiotopoulos for a system of interacting spheres that discretizing the spheres can lead to greater computational efficiency as compared to a real space simulation [38]. In the study by Panagiotopoulos, it was noted that a minimum of ten lattice sites was necessary to represent the sphere diameter in order to reproduce thermodynamic quantities consistent with real-space models. For the aspect ratios of rods studied here, we determined that a rod width must be represented by a minimum of ten lattice sites to produce equivalent results from a real-space simulation. Thus, all the rods studied here have a width of 10 and the length is adjusted to achieve the desired aspect ratio. For example, the rods with $\alpha=7.5$ have $D=10$ and $L=75$. One method to accelerate the test for overlap (to obtain U^{or}) is to render the rods hollow, as it is only necessary to check for overlap with points along the rod perimeter.

We also consider a discrete number of possible rod orientations. Recently, Shundyak and van Roij [39] calculated the equation of state for hard rods ($L \gg D$) for an increasing number of allowed orientations and compared their results to Onsager's continuum result. They showed that when greater than nine angles are allowed, the discrete solution begins to converge to the continuum solution and that the continuous Onsager result can be reproduced when greater than 50 angles are incorporated into the discrete model. They showed that as the density of rods is increased, an increasing number of rod orientations is required to reproduce the Onsager result. For $L > D$ (but not $\gg D$), it is expected that fewer rod orientations are required. Here, we allow for 180 different possible rod orientations, ranging from 0° to 179°, in one-degree increments. Thus, we expect our results to accurately reflect the continuum.

A simulation run consists of initialization, followed by equilibration and production runs. Most simulations were initialized by starting all rods with the same orientation but with random center-of-mass locations. For $A_f = 0.7$, we specified order to the centers of mass, as randomly placed centers of mass led to long initialization times because of the difficulty in locating free space to place all the rods. Following initialization, equilibration times ranged between 5×10^5 MC steps for the lowest area fractions to upwards of 10 million MC steps for $A_f = 0.7$. Here, a MC step is defined as an average of one attempted center-of-mass move per rod per step. To verify that the systems were adequately equilibrated, we checked for reproducibility of sampled quantities by performing several short production runs. We also initialized the simulations with rods having various different starting angles and center-of-mass distributions and obtained reproducible sampled quantities. Production runs for the bulk systems consisted of 7–10 runs ranging in length from $3.5 \times 10^5 - 7 \times 10^5$ MC steps. In the confined systems, 6–17 runs were conducted ranging in length from $5 \times 10^5 - 5 \times 10^6$ MC steps. The results reported below are obtained as averages over all production runs.

III. SIMULATION MEASURES

Several different measures were employed to characterize the ordering and phase behavior of our systems. A useful measure of the strength of the angular correlations between rods are the orientational correlation functions g_2 and g_4, which are given as ensemble averages $\langle \cdots \rangle$ by

$$g_2(r) = \langle \cos 2[\theta_i(0) - \theta_j(r)] \rangle \tag{5}$$

and

$$g_4(r) = \langle \cos 4[\theta_i(0) - \theta_j(r)] \rangle. \tag{6}$$

For bulk simulations, $\theta_i(0) - \theta_j(r)$ is the difference between the angles of rods i and j and r is the distance between the centers of mass of the rods. In the confined systems, $\theta_i(0)$ is the angle of the confining walls, which is taken to be 90°, and r is measured as the perpendicular distance from half a rod width behind the edge of the wall to the center of mass of the rod. By measuring r from behind the wall edge, we facilitate comparisons between confined and bulk systems. A value of g_2 or $g_4 = 1$ indicates that the rod angles are strongly correlated, while a value of g_2 or $g_4 = 0$ indicates that the rod angles are uncorrelated. When rods align parallel to one another (or to the wall), they contribute positively to both g_2 and g_4, whereas rods aligned perpendicular to each other (or to the wall) only contribute positively to g_4. In the bulk, g_2 is thus a measure of nematic correlations, whereas g_4 is a measure of tetratic correlations.

Another useful measure is the angular distribution function $P(\theta)$, which is given by

$$P(\theta) = \frac{\langle N(\theta) \rangle}{N_{\text{rods}} \Delta\theta}. \tag{7}$$

$P(\theta)$ is the probability of observing angle θ and $\langle N(\theta) \rangle$ is an ensemble average of the number of rods with an angle between θ and $\theta + \Delta\theta$. In the case of an isotropic phase, we expect the rods to adopt all possible orientations, resulting in a uniform distribution. In a nematic phase, where the orientational correlation lengths are larger than the box length, we expect that at any instant all the rods will have a similar orientation—although in the thermodynamic limit we also expect a uniform distribution for a nematic.

For the confined systems, the rod density profile $\rho(r)$ indicates the influence of the walls on rod positioning. This measure is given by

$$\rho(r) = \frac{\langle N(r) \rangle}{2H_{\text{box}} \Delta r}, \tag{8}$$

where $\langle N(r) \rangle$ is an ensemble average of the number of rods that have their center of mass at a distance between r and $r + \Delta r$ from the wall. As for g_2 and g_4, r is measured as the perpendicular distance from half a rod width behind the edge of the wall to the center of mass of the rod.

We calculate the nematic order parameter S from the order parameter tensor $\mathbf{Q}$ using

$$Q_{\alpha\beta} = \frac{1}{N_{\text{rods}}} \left\langle \sum_{i=1}^{N_{\text{rods}}} [2u_\alpha(i) u_\beta(i) - \delta_{\alpha\beta}] \right\rangle. \tag{9}$$

Here, $u_\alpha(i)$ and $u_\beta(i)$ are the αth and βth Cartesian coordinates of the unit vector specifying the orientation of rod i and $\delta_{\alpha\beta}$ is the Kronecker delta [14]. The largest eigenvalue of this 2×2 matrix is taken as the order parameter S. In a system with a high level of orientational order, such as the nematic phase, the order parameter will have high values with an upper limit of 1 for a perfectly aligned system. A system with a low level of orientational order, such as the isotropic phase, or systems in which high levels of orientational order persist over short distances, such as the tetratic phase, the order parameter with have a small value with a lower limit of zero.

IV. RESULTS

A. Bulk systems

We first present results from simulations of bulk systems. These results serve as a reference for the confined systems.

TABLE I. Phases observed in DFT calculations of rectangles [8] and MC simulations of DR [9], as well as values of the order parameter obtained using Eq. (9) from our simulations of bulk (S_{bulk}) and confined (S_{1L}–S_{10L}) rectangles.

A_f	α	DFT [8]	MC DR [9]	S_{bulk}	S_{1L}	S_{2L}	S_{5L}	S_{10L}
0.4	7.5	I	I	0.03	0.81	0.49	0.19	0.09
0.4	13.3	N_u	I/N_u	0.59	0.91	0.84	0.75	0.69
0.4	20.0	N_u		0.88	0.94	0.92	0.90	0.89
0.6	7.5	N_u	I	0.04	0.92	0.77	0.41	0.18
0.6	13.3	N_u	N_u	0.93	0.96	0.95	0.94	0.94
0.6	20.0	N_u		0.96	0.97	0.96	0.96	0.96
0.7	7.5	N_u	N_u	0.05	0.94	0.76	0.33	0.22
0.7	13.3	N_u	N_u	0.96	0.97	0.97	0.97	0.96
0.7	20.0	N_u		0.97	0.98	0.97	0.97	0.97

Further, there have been previous studies of two-dimensional hard rods that are relevant to our work. In particular, Martínez-Ratón *et al.* [8] used density-functional theory (DFT) based on scaled-particle theory to delineate a phase diagram for hard rectangles with various area fractions and aspect ratios. The authors noted two phases of rectangles that corresponded to our simulation conditions, the isotropic (I) and uniaxial nematic (N_u). Bates and Frenkel [9] used MC simulations to probe the phase diagram of hard discorectangles (DR)—the two-dimensional limit of spherocylinders—from the disk to needle limit. These results for α and A_f that overlap with ours, along with values of the order parameter S_{bulk} that we obtained using Eq. (9), are included in Table I.

For the α=13.3 and 20.0 at all three area fractions and α=7.5 at A_f=0.4, our results are in good agreement with the DFT [8] and MC DR [9] results. The high value of the order parameter for α=13.3 and 20.0 indicates a strong preference for uniaxial alignment indicative of the nematic phase. The small value of the order parameter for α=7.5 at A_f=0.4 is consistent with the isotropic phase. As can be seen for α=13.3 and 20.0, increasing the area fraction in the nematic phase leads to higher values of the order parameter as the rods adopt more angles in common.

The low value of the order parameter obtained for α=7.5 is in contrast with DFT results [8] for A_f=0.6 and 0.7 and contrasts MC DR results [9] for A_f=0.7. More insight into these bulk phases can be gained from the orientational correlation functions g_2 and g_4, which are shown in Fig. 2 for nematic and isotropic phases [Fig. 2(a)], as well as for α=7.5 and A_f=0.6 [Fig. 2(b)]. Similar results to those in Fig. 2(b) are seen for α=7.5 and A_f=0.7. As we see for the nematic in Fig. 2(a), both g_2 and g_4 retain high values over the entire distance range probed. This slow decay and the fact that $g_2 > g_4$ both reflect the predominately parallel alignment of the rectangles. On the other hand, for the isotropic phase [see Fig. 2(a)], both g_2 and g_4 decay rapidly to zero. If we look at g_2 and g_4 for α=7.5 at A_f=0.6 [Fig. 2(b)], we can see that g_4, a measure of tetratic correlations, dominates over longer distances than g_2, a measure of nematic correlations. This analysis indicates the possibility that the system is in a tetratic phase.

The possibility of a tetratic phase in two dimensions has been discussed in the literature. Although the DFT phase diagram in Ref. [8] does not predict the presence of the tetratic phase for α=7.5 at A_f=0.6 or 0.7, the authors note the presence of a metastable tetratic phase at shorter aspect ratios and higher area fractions. They note that they could not rule out the possibility of a stable tetratic phase. Experimental work on the ordering of cylinders on a two-dimensional surface reveals strong fourfold correlations, indicative of the tetratic phase, for α=5.2 and 12.6 at A_f=0.87 [15].

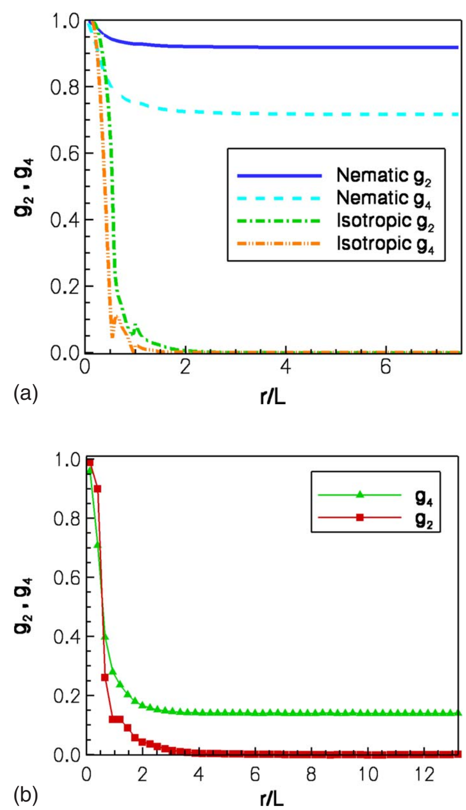

FIG. 2. (Color online) $g_2(r)$, given by Eq. (5), and $g_4(r)$, given by Eq. (6), as a function of rod center-of-mass separation for bulk systems with (a) α=13.3 and A_f=0.6, a nematic, and α=7.5 and A_f=0.4, an isotropic; and (b) α=7.5 and A_f=0.6.

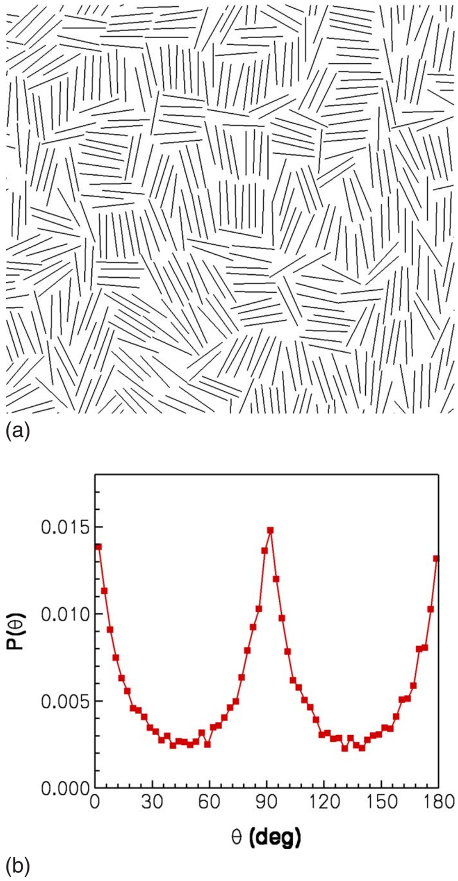

FIG. 3. (Color online) Characteristics of tetratic order for α =7.5 at A_f=0.6. (a) Snapshot from a bulk simulation. Here, the rectangles are represented by lines for clarity. (b) Angular distribution, given by Eq. (7).

A qualitative indication of tetratic order for α=7.5 at A_f =0.6 can be obtained from a snapshot for this system, shown in Fig. 3(a). Here, we note a tendency for the system to organize into perpendicular bundles of rods. The angular distribution of rods for this system, shown in Fig. 3(b), has peaks at 0°, 90°, and 180°, indicating tetratic tendencies. Finally, we obtained ensemble averages of g_2 and g_4 resolved in directions parallel and perpendicular to the long axis of a central rectangle. A similar method was used by Bates and Frenkel to study a system of spherocylinders with α=5 at a density of ρ=0.125D^{-2}, whose ordering was tetratic-like [9]. Figures 4(a) and 4(b) show g_2 and g_4 in the directions parallel and perpendicular to the long axis of a rectangle, respectively. In the parallel direction, Fig. 4(a), there is little structure to the rectangles, as can be seen from the nearly monotonic decay of g_2 and g_4. The peaks in the perpendicular direction [Fig. 4(b)] are spaced approximately one rod width apart, indicating small bundles of rods aligned with their long axes in parallel. It is interesting to note that in both the parallel and perpendicular directions the asymptotic value of g^4 is greater than g_2, as seen in Fig. 2(b). This is due to tetratic alignment of the rods. However, it is evident that this ordering is weak, as the overall magnitudes of g_2 and g_4 are small and the rod alignment persists only over small distances. Thus, we conclude that although the phases for

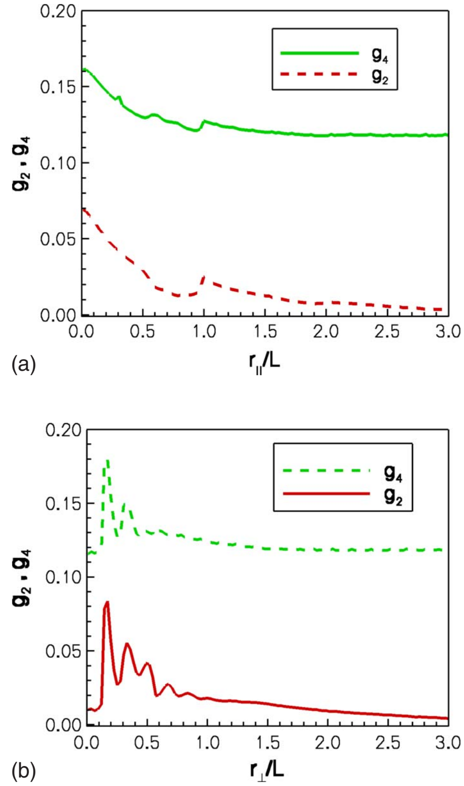

FIG. 4. (Color online) $g_2(r)$, given by Eq. (5), and $g_4(r)$, given by Eq. (6), as a function of (a) parallel and (b) perpendicular rod center-of-mass separation for α=7.5 at A_f=0.6.

α=7.5 with A_f=0.6 and 0.7 have characteristics of tetratic order, these are isotropic phases.

B. Confined systems

We will now discuss the results for the confined systems. Here, an overall measure of order is given by the order parameter S, which is included in Table I for all the wall separations studied. In Table I, we see, for a given area fraction, that the value of the order parameter increases as W_{box} decreases. As for the bulk systems, we see qualitatively similar trends for α=13.3 and 20.0 at all three area fractions. For these systems the rods align in a nematic phase in the bulk and under confinement. For α=7.5, the phase behavior of the rods depends on the wall separation and can differ from the bulk. The high values of S for short wall spacings with α =7.5 are characteristic of the nematic phase, but the value of S decreases toward the bulk (isotropic) value as W_{box} increases. While the value of the order parameter provides an indication of the net order in the confined systems, other measures more clearly indicate the influence of the walls. Below, we discuss these measures for the two different types of confined systems.

1. *Nematic in bulk and under confinement:* α=13.3 and 20.0. We first consider confined systems that exhibit nematic ordering in both the bulk and under confinement. As discussed above, rods with aspect ratios of 13.3 and 20.0 fall under this category for all area fractions. Representative

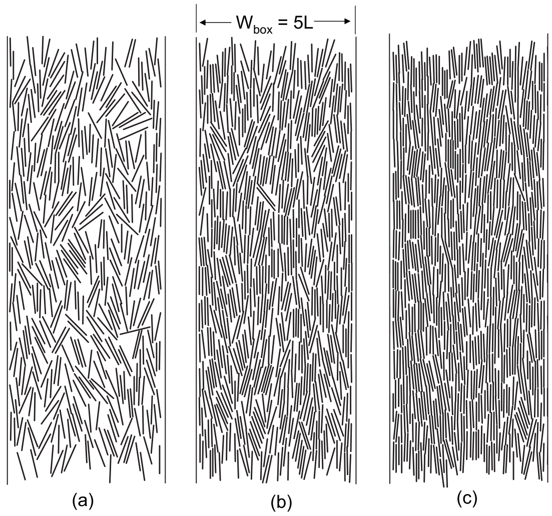

FIG. 5. Snapshots of confined systems with α=13.3, W_{box}=5L and (a) A_f=0.4, (b) A_f=0.6, and (c) A_f=0.7. The rods are shown as thin lines for clarity.

snapshots of three systems, with α=13.3, W_{box}=5L, and varying fractional coverage are shown in Fig. 5. These snapshots illustrate the trends that we will discuss below.

Figure 6 shows a plot of the orientational correlation function g_2 at conditions corresponding to the snapshots in Fig. 5. Here we see that at distances near 0, i.e., near the wall, the rods orient themselves parallel to the wall. As the rod-wall separation approaches the center of the confined region (i.e., half the box width), the rod-wall correlations are still strong for A_f=0.6 and 0.7, while there is some decay for A_f=0.4. The slow decay in g_2 indicates that under confinement the rods basically adopt the wall angle throughout the confined region, that is, the wall determines the nematic director. This is evident from the snapshots in Fig. 5 and stands in contrast to bulk nematics, for which the director is a random orientation that can change (slowly) with time.

Figure 7, which shows g_2 for all the confined and bulk systems having α=13.3 and A_f=0.4, indicates the influence of wall spacing on rod orientation. We note that Fig. 7 is

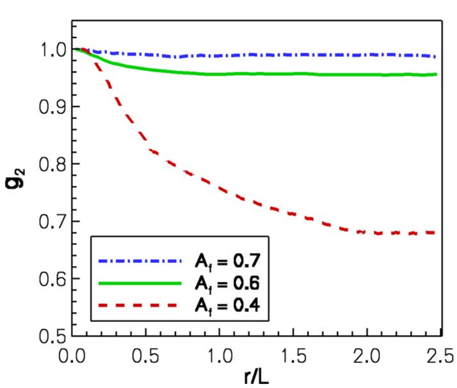

FIG. 6. (Color online) $g_2(r)$, given by Eq. (5), as a function of rod-wall separation distance. This plot shows the effect of increasing area fraction A_f in the confined region while holding constant the aspect ratio α=13.3 and wall spacing W_{box}=5L.

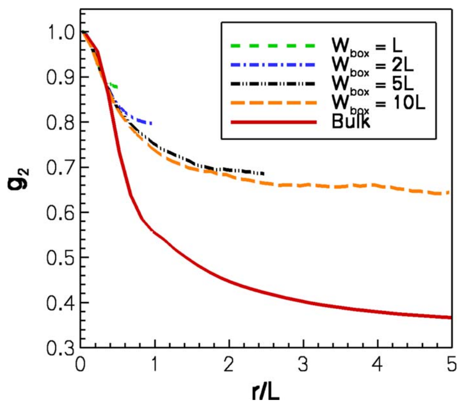

FIG. 7. (Color online) $g_2(r)$, given by Eq. (5), as function of rod center-of-mass separation (bulk system) and rod-wall separation (confined systems with W_{box}=1L–10L) for rods with α=13.3 and A_f=0.4.

representative of g_2 and g_4 for all area fractions. Here, we see that rods with the greatest confinement (smallest wall spacing) have the highest angular correlation near the center of the confined region and, for the wall spacings studied, this angular correlation is greater than we would see in the bulk. This reflects the fact that W_{box} is significantly smaller than the nematic correlation length for these systems. Thus, the parallel rod orientation set by the wall is largely preserved throughout the entire confined region.

Looking to small distances on Fig. 7, it is interesting to see that g_2 appears to exhibit a universal curve, which follows the bulk curve for sufficiently short rod-rod distances. This seems to indicate that angular correlations between two, closely spaced rods in the bulk are the same as those between a rod and an infinite wall. To further investigate this trend, we show g_2 for short rod-wall–rod-rod separations in Fig. 8. For A_f=0.4 [see Fig. 8(a)], we see that all the curves for the confined systems superimpose, but the bulk curve lies perceptibly above them at short separations. At higher rod densities (which are representative of A_f=0.6 and 0.7 for α=13.3 and 20.0), Fig. 8(b) shows that g_2 exhibits oscillatory behavior for the confined systems, but not for the bulk. It should be noted that such oscillations fall below the resolution of a plot such as Fig. 6, which shows g_2 for the entire confined region. These oscillations can lie above or below the bulk values and they reflect the layered structure that the walls impart to the rods. Thus, upon close inspection we see that g_2 does not follow a universal curve at close rod-rod–rod-wall separations.

Differences between the confined and bulk systems can be understood to arise from a combination of two effects: the density effect and the distance-sampling effect. As we see in Fig. 9(a), which shows the density profile for A_f=0.4 with α=13.3, the rod density exhibits a broad peak near the wall followed by a shallow minimum where the density is lower than the bulk value achieved near the center of the confined system. We note that over most of the distance range where g_2 for the bulk is greater than that for the confined system [see Fig. 8(a)], the density is lower for the confined system. Rods in a lower density region have more orientational free-

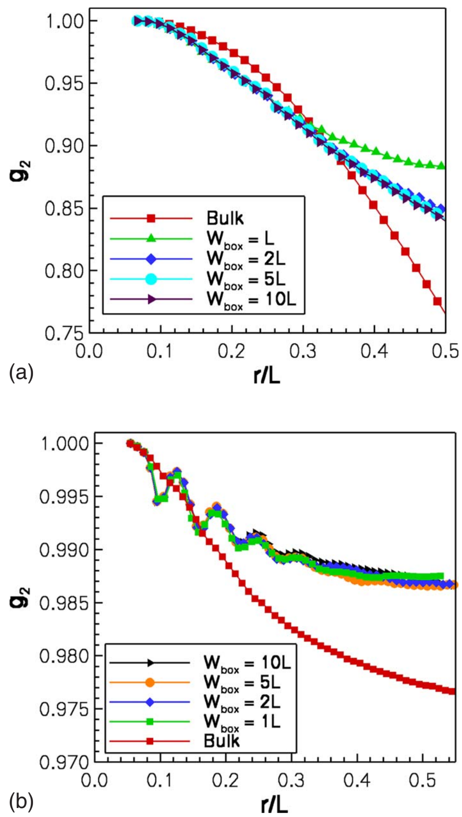

FIG. 8. (Color online) $g_2(r)$, given by Eq. (5), as function of rod center-of-mass separation (bulk system) and rod-wall separation (confined systems with $W_{\mathrm{box}}=1L-10L$) for rods with (a) $\alpha=13.3$ and $A_f=0.4$ and (b) $\alpha=20.0$ and $A_f=0.6$.

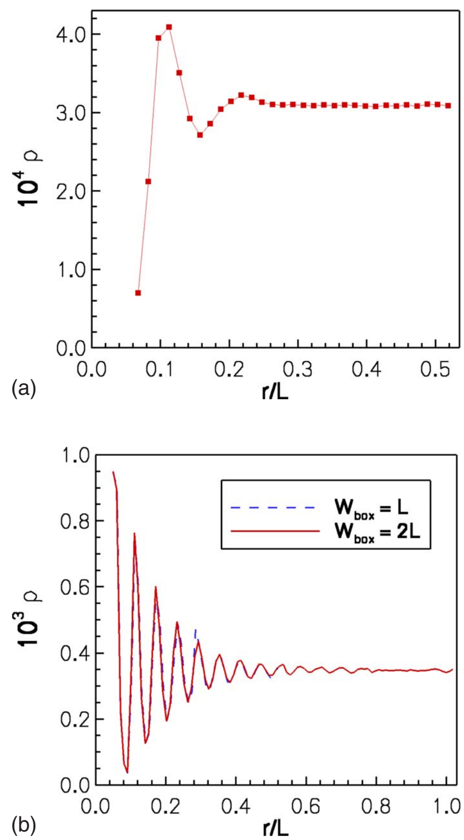

FIG. 9. (Color online) Rod density profiles, given by Eq. (8), as a function of rod-wall separation for $\alpha=13.3$ with (a) $A_f=0.4$ and $W_{\mathrm{box}}=1L$ and (b) $A_f=0.7$ with $W_{\mathrm{box}}=1L$ and $2L$.

dom and, thus, lower values of g_2. The density effect is more pronounced for higher overall rod densities [Fig. 8(b)], where the oscillatory structure of g_2 near the wall mirrors oscillations seen in the density profile. The density profile for $\alpha=20.0$ is shown in Fig. 9(b) for $A_f=0.7$, where we see strong oscillatory behavior with 13 peaks. The strong density oscillations reflect rod layering near the wall. For both $\alpha=13.3$ and 20.0 at $A_f=0.6$ we find that the rods form five layers of rods next to the wall. For $\alpha=13.3$ at $A_f=0.7$, nine layers occur. Interestingly, for the separations studied here, the degree of confinement does not appear to influence the rod density profiles near a wall as each of the profiles superimpose. Thus, wall-induced layering and its associated density variations can influence the value of g_2 close to a confining wall.

Although the above discussion has emphasized rod layering in the confined region, we note that rod layering also occurs in the high-density, bulk nematic phases for $A_f=0.6$ and 0.7. However, g_2 does not reflect this layering for the bulk systems [see Fig. 8(b)]. This is due to the "distance sampling" effect. In the confined systems, separations are measured as the perpendicular distance between a rod's center of mass and the wall, while in the bulk, separations are measured as the radial distance between the centers of mass of two rods. Thus, for a given rod-wall separation, there is only one possible configuration for a rod to have parallel alignment with the wall. In the bulk, however, the value of $g_2(r)$ reflects rods with perpendicular separations that can be less than r (when two rods have staggered ends) and, thus, it is not sensitive to local variations in density. Despite these differences, the differences between g_2 for the bulk and confined curves are small. For practical (engineering) purposes it is possible to predict the degree of rod alignment near a wall by inspection of bulk behavior.

Finally, we note that with regard to rod layering, the results that we find here differ from those observed in three-dimensional simulations of low-density spherocylinders in a slit-pore geometry [29]. In the study by Mao and colleagues [29], it was observed that rods with shorter aspect ratios had more pronounced layering in the vicinity of the wall than those with longer aspect ratios. This was attributed to the loss of rotational entropy near the wall being more significant in low density phases for longer rods. We found for the systems in this section that the layering is more extensive for the larger aspect-ratio rods and is due to the nematic nature of the bulk phases at the area fractions studied. Thus, the difference between our two-dimensional results and the three-dimensional results seems to be due to differences in density, rather than differences in dimensionality.

2. *Rod phase depends on confinement:* $\alpha=7.5$. In this section, we discuss results from simulations of confined rods with $\alpha=7.5$ at all three area fractions. From Table I, we see that the bulk phases are isotropic for this aspect ratio. For $A_f=0.4$, the bulk rods have no preference to align in any

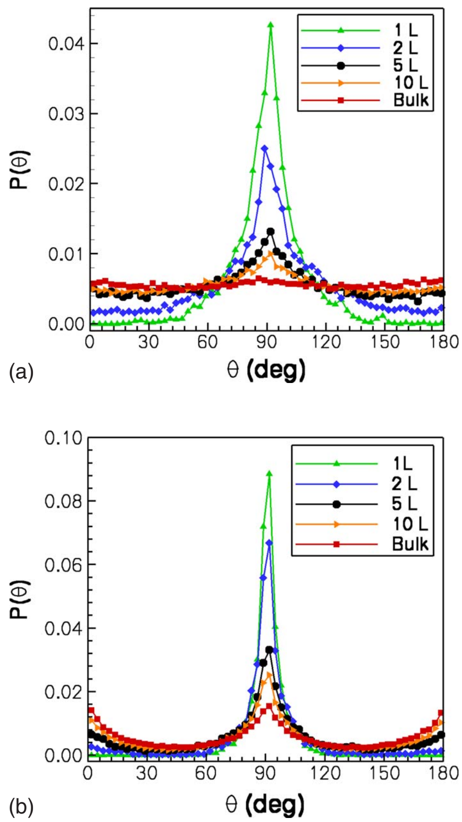

FIG. 10. (Color online) Angular distribution functions, given by Eq. (7), for α=7.5 (a) A_f=0.4 for bulk and W_{box}=1L–10L and (b) A_f=0.6 for bulk and W_{box}=1L–10L.

particular direction. As discussed above, rods with A_f=0.6 and 0.7 have a tetratic-like alignment, but do not possess the orientational and positional order of a tetratic phase. Table I shows that decreasing the wall separation for α=7.5 results in an increasing value of the order parameter, indicating the rods are aligning in a uniaxial manner. Below, we discuss the influence of the confining walls on rod ordering and how these bulk isotropic rods differ from the bulk nematics discussed above.

Figure 10(a) shows the angular distribution function for α=7.5 at A_f=0.4 and Fig. 10(b) shows the angular distribution function for A_f=0.6, which is similar to that for A_f=0.7. In Fig. 10(a), the bulk phase shows a flat line, which indicates the rods have no preference to align in any direction. As the separation between the walls is decreased to W_{box}=10L a small peak arises that is centered around θ=90°. This peak continues to sharpen as the spacing is further decreased, indicating the rods are collectively aligned parallel to the confining walls. In Fig. 10(b), we see that at a higher density, rods in the bulk phase exhibit a preference to align in perpendicular directions, which is shown by the peaks at 0°, 90°, and 180°. When these rods are confined to W_{box}=10L, their tetratic-like order persists but, compared to the bulk, a stronger peak occurs around θ=90°. As the confinement of the rods increases, the peak at θ=90° increases, while the peaks at θ=0° and 180° decrease. For W_{box}=1L, there is no indication of tetratic order and the rods exhibit a single peak centered around the angle of the confining wall.

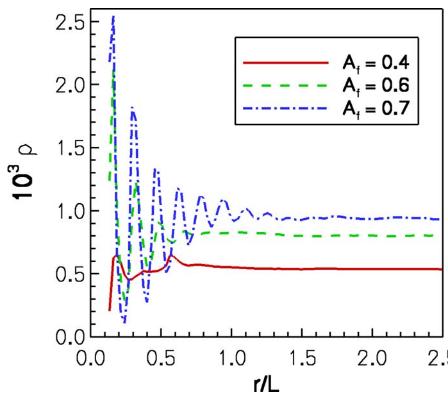

FIG. 11. (Color online) Rod density profiles, given by Eq. (8), as a function of rod-wall separation for α=7.5 at W_{box}=10L.

Thus, with increasing confinement, the bulk behavior of the rods is suppressed in favor of uniaxial alignment parallel to the wall. However, we do observe a tendency for the rods to be perpendicular to the wall and the remaining question we wish to answer is where (relative to the wall) we expect to find parallel and perpendicular rods.

Figure 11 shows the density profiles for α=7.5. Here, we show the density profiles for W_{box}=10L, truncated at r/L=2.5, and we note that the density profiles at the shorter wall separations are nearly identical. The density profile for A_f=0.4 in Fig. 11 exhibits two peaks. Although we also see two peaks at A_f=0.4 for rods with higher aspect ratios [see Fig. 9(a)], a significant difference occurs in the location of the peaks. While the rods with higher aspect ratios [Fig. 9(a)] align in two layers that are parallel to the wall (a layer that is approximately half a rod width away from the wall followed by a second layer that occurs approximately one rod width further), the rods with the lower aspect ratio (Fig. 11) exhibit a peak at approximately one rod width, indicating a parallel layer, followed by a small, second peak at half a rod length—the distance where we would expect to find a peak if rods were perpendicular to the wall. Upon increasing the density in the confined region (see Fig. 11), the peak at r/L=0.5 disappears and the density profiles for A_f=0.6 and 0.7 reflect several parallel layers of rods immediately adjacent to the confining walls. A similar shift in the location of the peaks in the density profile has also been observed for spherocylinders in three dimensions in the presence of a single hard wall [30], where the authors found that as the density of rods was increased, the location of the peak in the density profile shifted closer to the confining wall.

The orientational correlation functions shed more light onto the organization of rods near the confining walls. Figure 12 is a plot of g_2 for α=7.5 at A_f=0.4. A similar plot is obtained for g_4 but with smaller values, indicating that nematic correlations are more important than the tetratic correlations. With the exception of W_{box}=1L, all the plots for the confined systems show a slight peak near r/L=0.5—the distance where we observe the second peak in the density profile (Fig. 11). Because g_2 measures nematic correlations and this peak has higher values for g_2 than for g_4, we conclude that the rods at A_f=0.4 have a greater tendency to be parallel to wall at this distance. The absence of peaks at 0° and 180°

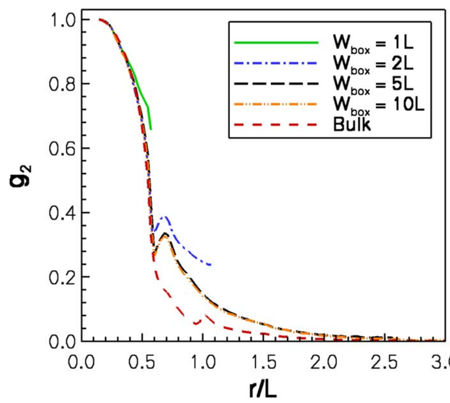

FIG. 12. (Color online) $g_2(r)$, given by Eq. (5), as function of rod center-of-mass separation (bulk system) and rod-wall separation (confined systems with $W_{box}=1L-10L$) for rods with $\alpha=7.5$ and $A_f=0.4$.

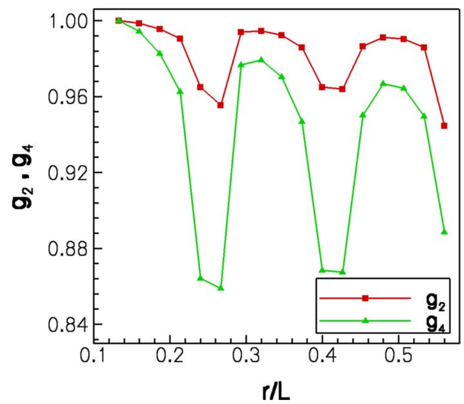

FIG. 14. (Color online) $g_2(r)$, given by Eq. (5), and $g_4(r)$, given by Eq. (6), as function of rod-wall separation with $W_{box}=1L$ for rods with $\alpha=7.5$ and $A_f=0.7$.

in the angular distribution in Fig. 10(a) confirms that there is no pronounced tendency for rods to be perpendicular to the walls. Thus, the relatively large spacing between the first and second peaks in the density profile in Fig. 11 reflects the weak organization of the rods as we move away from the wall.

Progressing to higher densities, Fig. 13 is plot of g_2 at $A_f=0.6$ and $W_{box}=5L$. From this plot, we see that close to the wall, g_2 is greater than g_4. Also, we observe oscillations in g_2 and g_4 that are spaced approximately one rod width apart, indicating parallel alignment of the rods with the wall. As we move away from the wall, a crossover occurs to a region where the rods assume bulk-like orientations [see Fig. 2(b)] and $g_4 > g_2$. The crossover of g_2 and g_4 occurs for $A_f=0.6$ and 0.7 at $W_{box}=2L$, $5L$ and $10L$. Only under the highest confinement (see Fig. 14) do nematic correlations dominate over the entire box width. We note that the wall spacing for which we observe a confined nematic ($W_{box}=1L$) corresponds to approximately twice the correlation length for g_2 for the bulk system, shown in Fig. 2(b). For $W_{box}=1L$, the center of the confined region is beyond the bulk correlation length from the wall and, thus, we observe bulk-like ordering

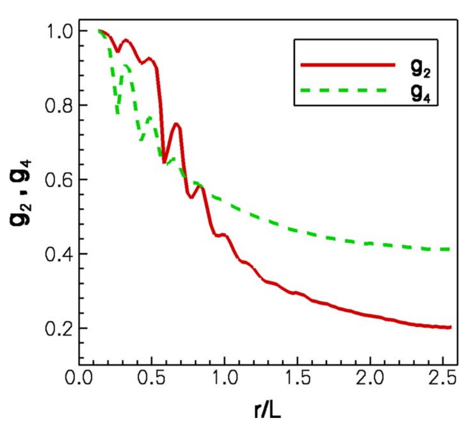

FIG. 13. (Color online) $g_2(r)$, given by Eq. (5), and $g_4(r)$, given by Eq. (6), as function of rod-wall separation with $W_{box}=5L$ for rods with $\alpha=7.5$ and $A_f=0.6$.

there. Thus, taken together with the density profiles (Fig. 11), Figs. 13 and 14 emphasize that near the walls, the rods align parallel to the walls, while the rods near the center of the confined region assume a bulk-like configuration. As the extent of the confined region decreases beyond twice the bulk correlation length for g_2, the tendency of the rods to align parallel to the walls increases. Different behavior was noted for spherocylinders in contact with a single hard wall and between two parallel hard walls in three dimensions. In these systems the confining wall induced a preference for the spherocylinders to have a biaxial alignment with the wall under certain conditions [30]. Although the biaxial phase observed in these three-dimensional studies cannot occur in two dimensions, it is nevertheless interesting that in both three dimensions and in our two-dimensional simulations, hard walls induce rod orientations that do not occur in the associated bulk. Biaxial alignment was observed where the bulk is, depending on density, either isotropic or nematic in three dimensions, and nematic alignment is observed here where a bulk tetratic-like phase occurs in two dimensions.

V. CONCLUSION

In summary, our studies demonstrate several effects of confinement for hard rectangles in two dimensions. For all of the rod aspect ratios and area fractions studied, we find that confinement induces the rods to align their long axes parallel to the walls. This increases the degree of nematic ordering over the bulk (indicated by the value of the nematic order parameter) to an extent that increases as the separation between the confining walls decreases. If the aspect ratio of the rectangles is sufficiently large (in our study, two aspect ratios $\alpha=13.3$ and 20.0 fall under this category), they exhibit nematic ordering in both the bulk and under confinement. We find that orientational correlations between these confined and bulk nematics are surprisingly similar for sufficiently close rod-wall or rod-rod separations. However, the hard, confining walls induce a subtle rod layering that is not observed in analogous bulk nematics. Rods with a small aspect ratio ($\alpha=7.5$) are isotropic in the bulk. For sufficiently high densities ($A_f=0.6$ and 0.7), these bulk rods exhibit weak tetratic-like ordering, but are still deemed to be isotropic. Under confinement, low-aspect-ratio rods become nematic, in the sense that their order parameters take on sufficiently large values. From studies of density profiles, angular distributions, and orientational correlation functions, it is apparent that the rods align their long axes parallel to the wall in the near-wall region, where layering occurs for the higher rod densities. However, the confined rods still exhibit weak tetratic (isotropic) tendencies near the center of the confined region for all but the smallest wall separations ($W_{\mathrm{box}}=1L$). We note that although our studies probe the ordering of hard rectangles, the entropic tendencies that we observe here will still be present for rods with energetic interactions, such as those functionalized by DNA [40–43] and polymer linkers [44,45]. Thus, these studies serve as a general starting point for understanding and controlling the assembly of rods in confining geometries.

ACKNOWLEDGMENTS

This work was funded by the National Science Foundation, Grants No. DGE-9987589 and No. CCR-0303976.

[1] D. Whang, S. Jin, Y. Wu, and C. M. Lieber, Nano Lett. **3**, 1255 (2003).
[2] R. Beckman, E. Johnston-Halperin, Y. Luo, J. E. Green, and J. R. Heath, Science **310**, 465 (2005).
[3] H. Ko and V. V. Tsukruk, Nano Lett. **6**, 1443 (2006).
[4] S. Liu, J. B.-H. Tok, J. Locklin, and Z. Bao, Small **2**, 1448 (2006).
[5] X. Chen, A. L. Rogach, D. V. Talapin, H. Fuchs, and L. Chi, J. Am. Chem. Soc. **128**, 9592 (2006).
[6] R. S. Mclean, X. Huang, C. Khripin, A. Jagota, and M. Zheng, Nano Lett. **6**, 55 (2006).
[7] M. C. McAlpine, H. Ahmad, D. Wang, and J. R. Heath, Nat. Mater. **6**, 379 (2007).
[8] Y. Martínez-Ratón, E. Velasco, and L. Mederos, J. Chem. Phys. **122**, 064903 (2005).
[9] M. A. Bates and D. Frenkel, J. Chem. Phys. **112**, 10034 (2000).
[10] A. Donev, J. Burton, F. H. Stillinger, and S. Torquato, Phys. Rev. B **73**, 054109 (2006).
[11] H. Schlacken, H.-J. Mögel, and P. Schiller, Mol. Phys. **93**, 777 (1998).
[12] J. A. Cuesta and D. Frenkel, Phys. Rev. A **42**, 2126 (1990).
[13] M. D. Khandkar and M. Barma, Phys. Rev. E **72**, 051717 (2005).
[14] D. Frenkel and R. Eppenga, Phys. Rev. A **31**, 1776 (1985).
[15] V. Narayan, N. Menon, and S. Ramaswamy, J. Stat. Mech.: Theory Exp. (2006), PO1005.
[16] L. Onsager, Ann. N. Y. Acad. Sci. **51**, 627 (1949).
[17] R. Blaak, D. Frenkel, and B. M. Mulder, J. Chem. Phys. **110**, 11652 (1999).
[18] B. S. John and F. A. Escobedo, J. Phys. Chem. B **109**, 23008 (2005).
[19] B. S. John, A. Stroock, and F. A. Escobedo, J. Chem. Phys. **120**, 9383 (2004).
[20] P. Bolhuis and D. Frenkel, J. Chem. Phys. **106**, 666 (1997).
[21] Z. Dogic and S. Fraden, Phys. Rev. Lett. **78**, 2417 (1997).
[22] D. Costa, F. Saija, and P. V. Giaquinta, J. Phys. Chem. B **107**, 9514 (2003).
[23] P. Yang, Nature (London) **425**, 243 (2003).
[24] P. Yang and F. Kim, ChemPhysChem **3**, 503 (2002).
[25] A. Tao, F. Kim, C. Hess, J. Goldberger, R. He, Y. Sun, Y. Xia, and P. Yang, Nano Lett. **3**, 1229 (2003).
[26] S. Lenhert, L. Zhang, J. Mueller, H. P. Wiesmann, G. Erker, H. Fuchs, and L. Chi, Adv. Math. **16**, 619 (2004).
[27] F. Kim, S. Kwan, J. Akana, and P. Yang, J. Am. Chem. Soc. **123**, 4360 (2001).
[28] Y. Martínez-Ratón, Phys. Rev. E **75**, 051708 (2007).
[29] Y. Mao, P. Bladon, H. N. W. Lekkerkerker, and M. E. Cates, Mol. Phys. **92**, 151 (1997).
[30] M. Dijkstra, R. van Roij, and R. Evans, Phys. Rev. E **63**, 051703 (2001).
[31] A. Chrzanowska, P. I. C. Teixeira, H. Ehrentraut, and D. J. Cleaver, J. Phys.: Condens. Matter **13**, 4715 (2001).
[32] A. Poniewierski and R. Hołyst, Phys. Rev. A **38**, 3721 (1988).
[33] J. Galanis, D. Harries, D. L. Sackett, W. Losert, and R. Nossal, Phys. Rev. Lett. **96**, 028002 (2006).
[34] D. de las Heras, E. Velasco, and L. Mederos, Phys. Rev. E **74**, 011709 (2006).
[35] M. Cosentino Lagomarsino, M. Dogterom, and M. Dijkstra, J. Chem. Phys. **119**, 3535 (2003).
[36] F. A. Escobedo and J. J. de Pablo, J. Chem. Phys. **106**, 9858 (1997).
[37] D. Frenkel and B. Smit, *Understanding Moleucular Simulation* (Academic, San Diego, 2002).
[38] A. Z. Panagiotopoulos, J. Chem. Phys. **112**, 7132 (2000).
[39] K. Shundyak and R. van Roij, Phys. Rev. E **69**, 041703 (2004).
[40] P. L. Biancaniello, A. J. Kim, and J. C. Crocker, Phys. Rev. Lett. **94**, 058302 (2005).
[41] G. P. Goodrich, M. R. Helfrich, J. J. Overberg, and C. D. Keating, Langmuir **20**, 10246 (2004).
[42] D. B. Lukatsky and D. Frenkel, Phys. Rev. Lett. **92**, 068302 (2004).
[43] C. A. Mirkin, R. L. Letsinger, R. C. Mucic, and J. J. Storhoff, Nature (London) **382**, 607 (1996).
[44] M. A. Horsch, Z. Zhang, and S. C. Glotzer, Phys. Rev. Lett. **95**, 056105 (2005).
[45] M. A. Horsch, Z. Zhang, and S. C. Glotzer, Nano Lett. **6**, 2406 (2006).